DC Readout in Enhanced LIGO

A Dissertation

Submitted to the Graduate Faculty of the
Louisiana State University and
Agricultural and Mechanical College
in partial fulfillment of the
requirements for the degree of
Doctor of Philosophy

in

The Department of Physics and Astronomy

by
Tobin Thomas Fricke
B.S., University of California, Berkeley, 2003
M.A., University of Rochester, 2005

August 2011

TABLE OF CONTENTS

Dedication

Acknowledgments

List of Tables

List of Figures

1. Introduction

1.1 Gravitational Waves

Almost all of humanity's knowledge of the universe is derived from observations of electromagnetic waves. The effort to detect gravitational waves seeks to expand this knowledge by observing an entirely different field, and to further verify the correctness of the theory of general relativity.

Any theory of gravity that avoids instantaneous action at a distance must feature some kind of gravitational waves. Even Newtonian gravity can be modified to account for propagation delays from massive bodies that are the sources of attraction[25]. Gravity as we know it, however, is described by the general theory of relativity. In general relativity, spacetime is treated as a four-dimensional manifold with some intrinsic curvature. This curvature is generated by the presense of mass and energy. In the absense of forces, particles follow geodesic trajectories on this manifold. Thus, in the quintessential words of John Wheeler(?), "Space tells matter how to move, matter tells space how to curve."

This relationship between matter and curvature is made formal through the Einstein field equation, which equates (up to units) the Einstein tensor (G), encoding curvature, with the Stress-Energy tensor (T), encoding the matter and energy contents:

$$\mathsf{G} = \frac{8\pi G}{c^4}\mathsf{T} \tag{1.1}$$

where G is (Newton's) universal gravitational constant and c is the speed of light.

To perform calculations, we typically need to work in some coordinate basis. Thus one will work with $G_{\mu\nu}$, where μ and $\nu \in 0, 1, 2, 3$ are coordinate indices. In this notation, the Einstein tensor is givenby $G_{\mu\nu} = R_{\mu\nu} - \frac{1}{2}Rg_{\mu\nu}$, where $R_{\mu\nu}$ is the Ricci curvature tensor, R is

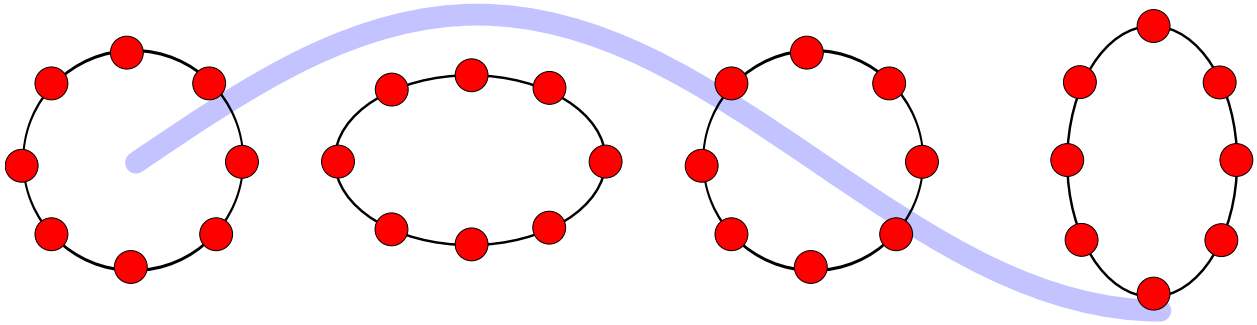

Figure 1.1: Depiction of the effect of a gravitational wave (traveling into the page) on a ring of non-interacting inertial test particles.

the Ricci scalar, and $g_{\mu\nu}$ is the spacetime metric. The metric plays a central role here, as it both encodes the curvature and implicitly defines the coordinate system.

To reveal the mechanism of gravitational waves, we are interested in vacuum ($\mathsf{T} = 0$) solutions of the Einstein field equations in the weak-field limit. In the weak-field limit, we can write the metric $g_{\mu\nu}$ as the sum of the flat-space Minkowski metric $\eta_{\mu\nu}$ and a small perturbation $h_{\mu\nu}$:

$$g_{\mu\nu} = \eta_{\mu\nu} + h_{\mu\nu}$$

This is the regime of linearized gravity. Calculating out the Einstein field equation keeping only terms of first-order in h and choosing the transverse-traceless gauge, one finds (see Sean Carroll's lucid exposition in [9] for the details) a wave equation for h:

$$\left(\nabla^2 - \frac{1}{c^2}\frac{\partial^2}{\partial t^2}\right) h_{\mu\nu} = 0$$

where $h_{\mu\nu}$ has, for a wave propagating along the z axis, the form:

$$[\mathsf{h}] = \begin{pmatrix} 0 & 0 & 0 & 0 \\ 0 & a & b & 0 \\ 0 & b & -a & 0 \\ 0 & 0 & 0 & 0 \end{pmatrix}$$

Here we see several of the essential points of gravitational waves:

- There are two independent components (polarizations)

- They travel at the speed of light
- They are manifest as a transverse tidal force on inertial objects

The amplitude of gravitational waves is quantified as the effective strain exerted on inertial test-masses.

1.2 The Hulse-Taylor Pulsar

Gravitational waves have not yet been directly detected, but very strong indirect evidence exists. Perhaps the strongest evidence is the Hulse-Taylor pulsar [17, 29]–a remarkable discovery of a binary star system in which one of the constituents is pulsar PSR B1913+16. The binary system is expected to radiate energy away into gravitational waves, causing its orbit to decay. The pulsar reveals the orbital parameters of the binary system, in particular its orbital period. Measurement of the orbital period through pulsar tracking over 30 years shows that the orbit is decaying exactly as predicted by general relativity.

Another binary system containing pulsars was discovered in 2004. In this system *both* objects are pulsars. [20, 19]

1.3 Sources of Gravitational Waves

Any system of mass accelerating in the quadrupolar or higher moments will radiate energy into gravitational waves. The effect is so weak, however, that only some of the universe's more cataclysmic events have a chance of producing waves observable on earth.

Anticipated sources of gravitational waves can be conveniently categorized as *continuous* or *transient*, and as *modeled* or *unmodeled*. There is some overlap in this division. Sources are paired with associated search efforts.

- **compact binary coalescence** — Pairs of compact objects (black holes or neutron stars) in binary orbits are expected to lose energy through gravitational waves, causing

the orbit to decay until the objects finally begin to interact and merge into a single object. This inspiral process will generate a characteristic chirp signal, followed by the complex merger process and then ringdown.

- **continuous wave** — Rapidly spinning objects will generate essentially monochromatic signals, which are in turn doppler-shifted by the relative motion of the Earth and the source. This is sometimes called the pulsar search, since the primary source in this category is expected to be rapidly spinning neutron stars (such as pulsars). The search, in turn, is divided into searches for known pulsars and unknown pulsars. Pulsars which are known electromagnetically can be targetted directly, whereas unknown pulsars require a brute-force search of the parameter space.

  Currently this is attacked in part through the distributed computing project Einstein@Home. One nicety of the pulsar search is that the process works equally well for analyzing radio telescope data–this has been done, resulting in the discovery of several previously unknown radio pulsars[18]. It is an open problem to find a more efficient search algorithm.

- **bursts** — Transient cataclysmic events such as supernovae will generate bursts of gravitational waves whose waveforms is not known in advance.

- **stochastic background** — In the same manner as the cosmic microwave background radiation, a cosmological background of gravitational waves is expected to exist. This is perhaps the most exotic anticipated source of gravitational waves, since its detection will inform us of the state of the universe at an age far earlier than has yet been probed. Sadly, the cosmological background is almost certainly too weak to detect in the forseeable future.

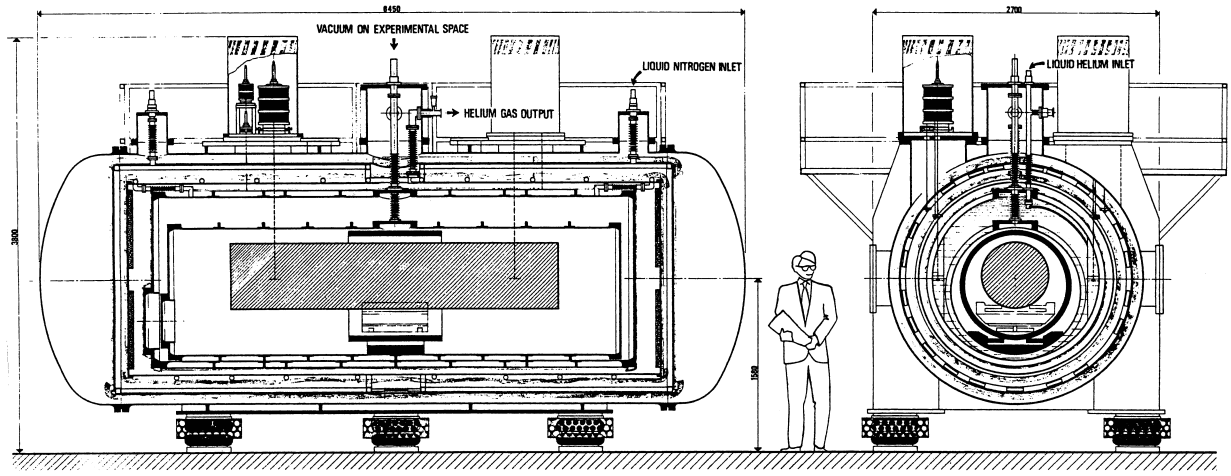

Figure 1.2: Depiction of the cryostat of the EXPLORER bar detector, which operated **somewhere** for **some time**. Illustration adapted from **a reference**.

The cacophony of unresolved astrophysical sources will also combine to produce a gravitational wave stochastic background.

The stochastic background search is fully coherent. In its simplest form, the search simply computes the correlation between pairs of gravitational wave detectors. This can be done in either an all-sky search or in a sky-position-dependent search. Typically, some power-law gravitational wave spectrum is assumed.

Improvements in search sensitivity can be achieved by incorporating knowledge of the expected signal waveform or spectrum; integrating over a long period of time (for continuous sources); and by looking for coincidence or coherence between multiple detectors.

The global network of gravitational wave detectors is operated as a sensor array, an interferometer composed of many interferometers.

1.4 Detectors

Gravitational waves couple to both light and matter.

The first attempts to detect gravitational waves used resonant bar detectors. In such a detector, a large cylinder of a metal alloy with a very high mechanical Q-factor is suspended in a vacuum chamber and cooled to cryogenic temperatures. A passing gravitational wave couples mechanical energy into the bar, ringing up the fundamental mechanical mode of the bar. Sensitive detectors (latter bars used SQUIDs) read out this mechanical displacement. Resonant bars are inherently narrow-band devices, sensitive to gravitational waves within a narrow linewidth about their fundamental resonance.

Bar detectors do have the advantage that they are small enough that they can be moved or re-oriented. The ALLEGRO bar detector at LSU was once rotated to modulate its overlap function with the nearby LIGO Livingston observatory.

1.4.1 Laser interferometers

Laser interferometers are now the instrument of choice in the search for gravitational waves. A gravitational wave will modulate the optical path length of light traveling transversely through it between inertial test masses. This path length modulation can be detected by a laser interferometer. The operation of laser interferometer gravitational wave detectors is the focus of this work and is detailed in the following chapters.

In terrestrial interferometers, large[1] glass cylinders serve as both super-polished mirrors and inertial test masses. These optics are hung as pendula to allow inertial freedom of the pendular resonance frequency.

References to cite in this section: [30, 12]

1.4.2 Other detectors

There are a few other mechanisms by which gravitational waves may be detected.

Pulsars serve as extremely reliable clocks, beaming a sequence of pulses towards earth whose arrival times can typically be predicted to better than a microsecond. The path

[1] 10 kg in Initial LIGO, 40 kg in Advanced LIGO

of the electromagnetic waves traveling from the pulsar to earth acts in some ways like an arm of a laser interferometer: gravitational waves passing transversely to the Earth-Pulsar baseline will modulate the optical path length, producing perturbations in the arrival time of the pulsar pulses–perturbations which are correlated between observations of distinct pulsars. Pulsar timing arrays seek to analyze these correlated residuals to find evidence of gravitational waves; Hobbs [16] anticipates that pulsar timing analysis will yield detections of gravitational waves in the nanohertz regime (period 3-30 years) in the next 5-10 years.

Primordial gravitational waves will also leave their imprint on the polarization of the cosmic microwave background radiation. Many CMB polarization experiments are currently under-way, searching for the faint "B-modes" in the microwave polarization.

1.5 The Future

It is hoped that Advanced LIGO, currently under construction, will bring the first direct detection of gravitational waves and begin the era of regular detection.

Several next-generation interferometers are in the works.

The Einstein telescope [2] is a planned system of three interferometers with arms forming an equilateral triangle, to be installed in tunnels deep under Europe.

In the meantime, technological development of terrestrial laser interferometers is a vibrant field. The Advanced detectors are anticipated to be limited almost everywhere by quantum mechanical noises, making gravitational wave detectors a verdant field for work in quantum optics. The next generation of terrestrial gravitational wave detectors will be limited by near-field gravity–"Newtonian noise" from density waves in the surrounding environment. The ways forward will be to move underground (where this effect is smaller); measure, predict, and subtract the Newtonian noise contribution using a seismic sensor array; or to move into space.

Going into space makes feasible the use of extraordinarily long arms and yields complete freedom from terrestrial noise, allowing access to very low frequency gravitational waves. The Laser Interferometer Space Antenna (LISA) design is composed of three spacecraft forming an equilateral triangle, the whole constellation in solar orbit. These spacecraft will house truly inertial test-masses, floating within an internal vacuum enclosure while external microthrusters keep the spacecraft centered around the test mass. The gravitational wave channel is derived using time-delay interferometery. The proposed LISA design is sensitive to gravitational waves in the range 10^{-4} to 10^{-1} Hz (period of 3 hours down to 10 seconds).

1.6 This Dissertation

This dissertation describes modifications to the initial LIGO detectors that were undertaken between 2008 and 2010. The state of the LIGO detectors before these modifications is described in [1] as well as numerous PhD dissertations, notably Rana Adhikari's [4] and and Stefan Ballmer's [6]. Robert Ward's dissertation details the implementation and evaluation of DC readout at the LIGO 40 meter prototype interferometer in Pasadena [28].

This dissertation does not address angular controls.

2. The LIGO detector

2.1 Arms, cavities, etc

By a convenient coincidence, a Michelson interferometer is ideally suited to gravitational wave detection. A suitably polarized wave directly excites the differential mode of the Michelson, while the Michelson simultaneously provides huge level of common mode noise rejection.

[14]

2.2 Interferometer Sensing and Control

The laser light incident on the interferometer is phase-modulated at several frequencies, producing optical sidebands on the laser carrier. Light extracted from the interferometer at its various ports is incident on photodiodes; the photodiode signals are demodulated to produce signals.

2.3 The Pound-Drever-Hall technique

The phase modulation may be expanded in terms of sidebands using the Jacobi-Anger expansion:

$$\begin{array}{rcll} \exp\{i\Gamma\cos\Omega t\} & = & \sum_{n=-\infty}^{\infty}(i^n) & J_n(\Gamma)\exp\{in\Omega t\} \\ \exp\{i\Gamma\sin\Omega t\} & = & \sum_{n=-\infty}^{\infty} & J_n(\Gamma)\exp\{in\Omega t\} \end{array} \tag{2.1}$$

2.4 Summary of changes made for Enhanced LIGO

After the successful completion of the Initial LIGO science goals, it was decided [5, 13, 26] to attempt to further improve the detector sensitivity by aggressively implementing a few prototype Advanced LIGO technologies.

Changes included:

- Fancy new laser
- Renovation of the input optics to handle higher power operation, including new electro-optic modulators [23]
- Installation of an output mode cleaner, supported by a prototype of the advanced LIGO in-vacuum seismic isolation system
- New Thermal Compensation System to handle the higher power

DC readout has been implemented previously at the Caltech 40 meter prototype [27, 28] and the GEO 600 detector[15, 22, 10]. The current configuration of Virgo incorporates an output mode cleaner but uses RF heterodyne readout[3].

2.5 History of the noise during Enhanced LIGO

2.6 Future directions

3. DC Readout - Theory of Operation

3.1 Introduction

The basic problem is to detect optical phase. Detectors are generally much too slow to detect the optical field *amplitude* directly (a laser wavelength of 1064 nm corresponds to about 3 THz). Instead, photodetectors measure the field *power*, averaged over some interval (typically MHz). To sense the optical phase, we turn to interference. By providing a second optical field–a *local oscillator*–as a phase reference, phase perturbations of the signal beam are converted to power fluctuations at the photodiode.

If the local oscillator is at the same optical frequency as the signal beam, then the photocurrent directly mimics the phase perturbations of the signal; this is *homodyne detection*, or direct conversion. If, on the other hand, the local oscillator offset slightly in frequency, the signal will appear as amplitude modulation on the photodiode signal. This is *heterodyne detection*.

There is also the question of how to get the local oscillator to the detection photodiode, and how to guarantee that it is sufficiently stable in phase, and well-matched to the spatial distribution of the signal beam. One approach is to specially pipe the local oscillator to the detection port, combine the signal and local oscillator via a beamsplitter, and detect the two emerging beams on photodiodes, adding the resulting signals electronically. This scheme, balanced homodyne detection, is depicted in **a figure**.

The problem is elegantly addressed in the current gravitational wave detectors by having the local oscillator signal resonate in the the interferometer, or a portion of it.

3.2 Interferometer Sensing and Control

The laser light incident on the interferometer is phase-modulated at several frequencies, producing optical sidebands on the laser carrier. Light extracted from the interferometer at its various ports is incident on photodiodes; the photodiode signals are demodulated to produce signals.

3.3 Heterodyne detection

In the context of coupling lasers to resonant cavities, heterodyne detection is known as the Pound-Drever-Hall technique. The canonical reference is [11], while [7] provides a pedagogical introduction.

3.3.1 The Pound-Drever-Hall technique

The phase modulation may be expanded in terms of sidebands using the Jacobi-Anger expansion:[1]

$$\begin{array}{rcll} \exp\{i\Gamma\cos\Omega t\} & = & \sum_{n=-\infty}^{\infty}(i^n) & J_n(\Gamma)\exp\{in\Omega t\} \\ \exp\{i\Gamma\sin\Omega t\} & = & \sum_{n=-\infty}^{\infty} & J_n(\Gamma)\exp\{in\Omega t\} \end{array} \tag{3.1}$$

Upon reflection from a cavity the phases of the carrier and the two sidebands will be rotated. This phase rotation converts the phase modulation to amplitude modulation, which is observed by the photodiodes. Typically, the carrier is held on resonance, where there is a very large change in reflected phase for a small change of detuning; the sidebands, on the other hand, are typically far from resonance and experience very little phase change.

The reflectivity of a lossless Fabry-Perot cavity is:

$$r_c = \frac{r_1 - r_2\exp i2\phi}{1 - r_1 r_2\exp i2\phi} \tag{3.2}$$

Suppose the carrier and upper and lower sidebands are incident upon this cavity, and the reflection from the cavity is incident on a photodiode. If the cavity length is L and the

[1] This expansion comes from the generating function $\exp\{\frac{1}{2}z\left(t-t^{-1}\right)\} = \sum_{m=-\infty}^{\infty} t^m J_m(z)$ with $t = \exp\{i\omega t'\}$

optical frequency is ν then $\phi = (2\pi)(L/c)\nu$. The sideband detunings are offset from this by $\pm(2\pi)(L/c)\Omega$. So, as a function of detuning, we have:

$$E_r = J_0 r_c(\phi) + J_1 r_c(\phi - (2\pi L/c)\Omega) + J_1 r_c(\phi + (2\pi L/c)\Omega) \tag{3.3}$$

...

Now consider a Michelson interferometer where the arms have lengths $L_{\{x,y\}}$. The field at the output port (at a given frequency) is:

$$E_{AS} = E_0 \frac{1}{2}\left(e^{2iL_x\nu/c} + e^{2iL_y\nu/c}\right) \tag{3.4}$$

3.4 Homodyne detection

DC readout creates a homodyne local oscillator by putting a small offset into the Michelson or DARM degree of freedom, moving the interferometer slightly off of the DARM fringe at DC. In this "fringe" view, the operation is very simple to understand: moving off of the null point introduces a non-zero first derivative. The limitation of this view is that it is awkward to include frequency-dependent effects, such as the finite storage time of the arms.

The true beauty of this technique is that the laser carrier that does leak out of the output port has been filtered by the combined action of the power recycling cavity and the arm cavities. Although by moving off of the dark fringe we do subject ourselves to some first-order coupling of common-mode noises, this filtering action (combined with having a sufficiently quiet laser to start with) reduces these noises below the fundamental noise floor of the detector.

As long as the DARM offset is sufficiently small, the degradation of power recycling is negligible.

3.4.1 Calculation of the optical gain

To the extent that the introduction of DC offset simply creates a nonzero carrier field at the output port and does not otherwise affect the interferometer dynamics, the frequency response of the interferometer is the same in DC readout as in heterodyne readout, except for an overall scaling. This can be seen by considering the sideband picture (see Figure **figure**) and is borne out by the following derivation.

3.4.2 Calculation of the optical gain

To the extent that the introduction of DC offset simply creates a nonzero carrier field at the output port and does not otherwise affect the interferometer dynamics, the frequency response of the interferometer is the same in DC readout as in heterodyne readout, except for an overall scaling. This can be seen by considering the sideband picture (see Figure **??**) and is borne out by the following derivation.

The optical gain for slow variations of the differential arm length can be found by calculating the power at the output port as a function of differential arm displacement and taking the derivative. The frequency response within the detection band is put in by hand. (Is there a nice way to do this in a frequency-dependent manner?)

The amplitude transmission coefficient of a Michelson interferometer is:

$$t_M = \frac{1}{2}\left(r_x\left(\phi_x\right) - r_y\left(\phi_y\right)\right) \tag{3.5}$$

where r_x and r_y are the amplitude reflectivity coefficients of the arms with detunings ϕ_x and ϕ_y.

We adopt a change of variable $\phi_- = \phi_x - \phi_y$, $\phi_+ = \frac{1}{2}\left(\phi_x + \phi_y\right)$.

For an interferometer with perfectly reflective arms, we have

$$t_M = \frac{1}{2}\left(e^{i\phi_x} - e^{i\phi_y}\right) = \frac{1}{2}\left(e^{+i\phi/2} - e^{-i\phi/2}\right) = i\sin\frac{\phi_-}{2} \tag{3.6}$$

The power at the output port is

$$P_{AS} = P_{BS} \sin^2\left(\frac{\phi_-}{2}\right) \tag{3.7}$$

The differential phase is equal to the wavenumber $k = (2\pi)/\lambda$ multiplied by the differential displacement x multiplied by the phase gain of the cavity and an additional factor of two, since a simple displacement of an end mirror causes 2x path length change. For a cavity with amplitude reflectivity $r_c(\phi)$, this phase multiplier is:

$$M(\phi) = \text{Im}\ \frac{1}{r_c(\phi)} \frac{\partial}{\partial \phi} r_c(\phi) = \text{Im}\ \frac{r_c'}{r_c}$$

giving:

$$\phi_- = 2kMx_-$$

So the output power is

$$P_{AS} = P_{BS} \sin^2 kMx_- \tag{3.8}$$

The optical gain at for slow differential motion is simply the derivative of P_{AS}. Here we assume that the change of P_{BS} and the phase gain M are negligible:

$$S_{DC} = \frac{dP_{AS}}{dx_-} = P_{BS} 2kM \cos() \sin() \tag{3.9}$$

For convenience we can write this in terms of P_{AS}:

$$S_{DC} = 2\sqrt{P_{BS} P_{AS}} Mk \cos\left(kMx_-\right) \tag{3.10}$$

The cosine term is very near unity and can be neglected. We write the power at the beamsplitter in terms of the carrier amplitude recycling gain g_{CR} and the power at the input to the interferometer: $P_{BS} = g_{CR}^2 P_{IN}$. So we get:

$$S_{DC} = 2\sqrt{P_{IN} P_{AS}} g_{CR}(\Delta x) M(k\Delta x + \omega) \tag{3.11}$$

Figure **??** compares this analytic expression to results obtained via a numerical modelling with Optickle. Agreement within the LIGO detection band is excellent.

Better expression for P_{AS}

We can substitute $\phi = \phi_x = -\phi_y$ since we're interested in differential motion of the arms, and substitute the Fabry-Perot reflection coefficient:

$$r_c(\phi) = \frac{r_1 - r_2 e^{i2\phi}}{1 - r_1 r_2 e^{i2\phi}} \tag{3.12}$$

where $\phi = kx$ is the one-way phase accumulated in the arm, r_1 is the reflectivity of the ITM, and r_2 is the reflectivity of the ETM.

Working out t_M for differential arm displacement, we find:

$$t_M = i r_2 g^2 \frac{\sin 2\phi}{1 + F \sin^2 \phi} \tag{3.13}$$

where g is the amplitude gain of the arm cavities and F is their coefficient of finesse. Taking the modulus-squared of this, and then multiplying by the incident power, we get the power at the output port:

$$P_{AS}(\phi) = P_{BS}(\phi) R_2 \frac{g^4}{\left(1 + F \sin^2 \phi\right)^2} \sin\phi \cos\phi \tag{3.14}$$

[steps omitted]

Taking the derivative with respect to δx, we find the optical gain, in Watts/meter, as:

$$S_{DC} \approx 2\sqrt{P_{IN} P_{AS}}\, g_{cr} r_{cp} k \tag{3.15}$$

3.5 Comparison

In addition to mitigating technical difficulties of RF detection, homodyne detection confers a fundamental improvement in SNR by up to a factor of ??. The extra noise in heterodyne detection can be considered either a result of time dependence in the average power leading to correlations in the shot noise[21], or the simple fact that demodulation introduces noises

from around $2f_{mod}$, giving an extra dose of shot noise. A more sophisticated analysis ascribes this noise to the two heterodyne demodulation quadratures acting as non-commuting quantum operators[8].

4. Output Mode Cleaner

4.1 Introuction

The interferometer has many degrees of freedom (both longitudinal and angular). We elect only to use DC readout for the DARM degree of freedom and continue to use heterodyne readout for (most of) the other degrees of freedom. Therefore we still require the sidebands to sense these degrees of freedom, so we can't simply turn them off. Instead we introduce an *output mode cleaner* at the output port in order to remove them there.

4.2 Physical design of the cavity

The output mode cleaner (OMC) consists of a four-mirror bowtie cavity with a finesse of approximately 350. The cavity optics and detection photodiodes are attached to tombstones which are bonded to a glass slab. This entire optical bench is suspended by a double pendulum, which in turn rests on an active seismic isolation platform, all of which is contained within the vacuum envelope. For convenience the chamber containing the OMC is isolated from the rest of the LIGO vacuum envelope via a septum window, allowing the independent venting of this chamber for easier access.

The output of the OMC is split via a 50/50 beamsplitter and directed onto two high-quantum-efficiency InGaAs photodiodes. The two photodiode signals allow the formation of sum and difference signals, the difference providing a diagnostic 'nullstream'.

4.3 Requirements

The OMC is required to sufficiently filter the light present at the output port such that contributions from the RF sidebands and higher-order spatial modes become negligible. To

exclude the RF sidebands, the cavity length is chosen such that the RF sideband frequencies are anti-resonant in the cavity, which yields minimum transmission.

4.4 Length control

4.5 Input beam control (ASC)

4.6 Automatic gain control

4.7 Residual fluctuations

4.8 Optical characterization

4.8.1 Mode scan

With the interferometer controlled using the heterodyne readout, the Output Mode Cleaner can be used as a mode analyzer cavity by varying the cavity length by at least a free-spectral-range. Because this range is more than the fast PZT actuator, this is accomplished by putting a large step into the thermal actuator. These mode scans can address questions such as:

- How well aligned is the OMC?
- How well mode-matched is the OMC?
- How much carrier power is at the output port compared to sideband power?
- How well balanced are the RF sidebands?
- How much junk light is present at the output port?
- Are there any nasty modes near the 00 mode that will sneak through?

- The horizontal/vertical mode separation

The mode scan cannot, by itself, distinguish carrier mode light from the arms vs carrier mode junk light.

4.8.2 Scattering

4.9 Interferometer lock acquisition

Initial lock acquisition of the Enhanced LIGO interferometers is the same as in Initial LIGO. Once the interferometer is locked using the heterodyne readout schemes, a DARM offset is introduced to allow carrier light to be transmitted to the output port. The Output Mode Cleaner is then locked to this carrier light. Once the OMC is locked to the carrier, control of DARM is transferred to the DC readout system. After this transition, a few other changes are made to engage the OMC alignment servoes and to put the readout electronics into low noise mode. At this point the interferometer has reached its operation configuration and astrophysical data-taking ("science mode") begins.

4.10 Beam diverter

When the interferometer loses lock, the stored power must be dumped somewhere. Typically, due to the presence of the power recycling mirror, the stored power comes out the output port. This high-power transient is sufficiently strong to burn the detection photodiodes. In order to prevent this, one of the steering mirrors is used as a fast shutter. It is able to zero the transmission through the OMC in approx 2 ms.

5. DC readout - evaluation

5.1 Noise couplings - modeled and measured

The coupling of noises from the laser source and RF oscillators to the gravitational wave readout channel differ considerably in RF and DC readouts. In addition, DC readout with an OMC is generally much more sensitive to beam motion (jitter). These couplings are of primary interest in designing the optical readout of a gravitational wave detector.

5.1.1 Laser frequency noise

5.1.2 Laser intensity noise

5.1.3 Oscillator amplitude noise

Reduced coupling of noises from the RF oscillator is one of the motivations for implementing DC readout. Despite not relying on the sidebands directly, behavior of the RF oscillator is still able to sneak into the DC readout.

One coupling path is conversion of Oscillator AM to laser intensity AM via the RF modulator. The sideband RIN per oscillator AM is given by

$$2\Gamma_0 \frac{J_1'(\Gamma_0)}{J_1(\Gamma_0)} = \Gamma_0 \frac{J_0 - J_2}{J_1}$$

(see Livingston elog 2010-07-15, "sideband RIN per oscillator AM calculation,").

Measured coupling is shown in figure **??**.

5.1.4 Oscillator phase noise

Oscillator phase noise sneaks in via some dirt effect. Look at how much better it is in DC readout!

Measured coupling of oscillator phase noise to the readout channel is shown in figure **??**.

5.1.5 Beam jitter noise

Beam jitter noise is perhaps the most important new noise source in DC readout and is tied to alignment of the OMC, which has proved to be one of the most subtle new issues. The output mode cleaner converts motion of the input beam into variations in transmission. The resulting variation in the transmitted light level is indistinguishable from DARM motion.

5.1.6 Electronics noise

The DC readout system provides a quantum-limited readout at $\sim$ 100 Hz. Careful engineering ensures that we are not limited by electronics thermal noise or $1/f$ flicker noise.

5.1.7 Optical spring

Detuning the arm cavities from their resonance introduces a big optical spring. This doesn't seem to have any measurable effect.

5.1.8 Nonlinearity of the DC error signal

Although we operate sufficiently far from the dark fringe that the linear coupling of residual DARM motion to output power is dominant, sufficiently large motion could produce second-order coupling. Fortunately, this turns out to be totally negligible.

5.2 Noise budget

5.3 Optical gain

6. Advanced LIGO

6.1 TBD

6.1.1 TBD

7. Appendix

7.1 The difference between PM and AM

Suppose we have a signal consisting of a carrier (at frequency ω and with unit amplitude) and two sidebands, of amplitudes a (lower) and b (upper), separated from the carrier by a frequency Ω:

$$E(t) = (1 + a\exp(-i\Omega t) + b\exp(i\Omega t))\exp(i\omega t) \tag{7.1}$$

To find the power in this signal, we take the modulus squared, $P = E^*E$ where * is the complex conjugate:

$$\begin{aligned} P = &\left(1 + |a|^2 + |b|^2\right) \\ &+ (a^* + b)\exp(-i\Omega t) + (a + b^*)\exp(i\Omega t) \\ &+ (ab^*)\exp(-2i\Omega t) + (a^*b)\exp(2i\Omega t) \end{aligned} \tag{7.2}$$

The condition for the 1Ω variation in the power to vanish is $a = -b*$, i.e. the real parts of the amplitudes of the sidebands must be opposite, and the imaginary parts must be equal. So we can extract the amplitude and phase modulation indicies:

$$\begin{aligned} m_{AM} &= (a + b^*) \\ m_{PM} &= (a - b^*) \end{aligned} \tag{7.3}$$

What is the condition for the 2Ω signal to vanish? With just two sidebands, it will always be present (though at second order in the sideband amplitude). In true phase modulation, the 2Ω signal is cancelled by the interaction of (the infinite number of) higher-order sidebands. As best I can tell, there is no simple arrangement of this cancellation other than via a magical property of the Bessel functions.

7.2 Optical phase conventions

7.3 The optical spring

7.4 Control theory basics

Operation of the LIGO detectors relies crucially on feedback control systems. In general, the response of the optical plant is very nonlinear; in order to produce a valid readout, the plant must be held very close to its operating point.

7.5 References

[24]

Bibliography

[1] B. P. Abbott and et al. LIGO: the Laser Interferometer Gravitational-wave Observatory. *Reports on Progress in Physics*, 72(7):076901+, July 2009.

[2] M. Abernathy and Others. Einstein Telescope Design Study. Technical report, Einstein Telescope Science Team, May 2011.

[3] F. Acernese and et al. The Virgo 3 km interferometer for gravitational wave detection. *Journal of Optics A: Pure and Applied Optics*, 10(6):064009+, June 2008.

[4] Rana Adhikari. *Sensitivity and noise analysis of 4 km laser interferometric gravitational wave antennae*. PhD thesis, Massachusetts Institute of Technology, July 2006.

[5] Rana Adhikari, Peter Fritschel, and Sam Waldman. Enhanced LIGO. Technical Report T060156-01-I, LIGO Laboratory, July 2006.

[6] Stefan Ballmer. *LIGO interferometer operating at design sensitivity with application to gravitational radiometry*. PhD thesis, Massachusetts Institute of Technology, June 2006.

[7] Eric D. Black. An introduction to Pound–Drever–Hall laser frequency stabilization. *American Journal of Physics*, 69(1):79–87, January 2001.

[8] Alessandra Buonanno, Yanbei Chen, and Nergis Mavalvala. Quantum noise in laser-interferometer gravitational-wave detectors with a heterodyne readout scheme. *Physical Review D*, 67(12):122005+, June 2003.

[9] Sean M. Carroll. Lecture Notes on General Relativity. December 1997.

[10] J. Degallaix, H. Grote, M. Prijatelj, M. Hewitson, S. Hild, C. Affeldt, A. Freise, J. Leong, H. Lück, K. A. Strain, H. Wittel, B. Willke, and K. Danzmann. Commissioning of the tuned DC readout at GEO 600. *Journal of Physics: Conference Series*, 228(1):012013+, May 2010.

[11] R. W. P. Drever, J. L. Hall, F. V. Kowalski, J. Hough, G. M. Ford, A. J. Munley, and H. Ward. Laser phase and frequency stabilization using an optical resonator. *Applied Physics B: Lasers and Optics*, 31(2):97–105, June 1983.

[12] Robert L. Forward. Wideband laser-interferometer graviational-radiation experiment. *Physical Review D*, 17(2):379–390, January 1978.

[13] Peter Fritschel, Rana Adhikari, and Rai Weiss. Enhancements to the LIGO S5 Detectors. Technical Report T050252-00-I, LIGO Laboratory, November 2005.

[14] Peter Fritschel, Rolf Bork, Gabriela González, Nergis Mavalvala, Dale Ouimette, Haisheng Rong, Daniel Sigg, and Michael Zucker. Readout and Control of a Power-Recycled Interferometric Gravitational-Wave Antenna. *Appl. Opt.*, 40(28):4988–4998, October 2001.

[15] S. Hild, H. Grote, J. Degallaix, S. Chelkowski, K. Danzmann, A. Freise, M. Hewitson, J. Hough, H. Luck, M. Prijatelj, K. A. Strain, J. R. Smith, and B. Willke. DC-readout of a signal-recycled gravitational wave detector. *Classical and Quantum Gravity*, 26(5):055012+, March 2009.

[16] G. Hobbs, A. Archibald, Z. Arzoumanian, D. Backer, M. Bailes, N. D. R. Bhat, M. Burgay, S. Burke-Spolaor, D. Champion, I. Cognard, W. Coles, J. Cordes, P. Demorest, G. Desvignes, R. D. Ferdman, L. Finn, P. Freire, M. Gonzalez, J. Hessels, A. Hotan, G. Janssen, F. Jenet, A. Jessner, C. Jordan, V. Kaspi, M. Kramer, V. Kondratiev, J. Lazio, K. Lazaridis, K. J. Lee, Y. Levin, A. Lommen, D. Lorimer, R. Lynch, A. Lyne, R. Manchester, M. McLaughlin, D. Nice, S. Oslowski, M. Pilia, A. Possenti, M. Purver, S. Ransom, J. Reynolds, S. Sanidas, J. Sarkissian, A. Sesana, R. Shannon, X. Siemens, I. Stairs, B. Stappers, D. Stinebring, G. Theureau, R. van Haasteren, W. van Straten, J. P. W. Verbiest, D. R. B. Yardley, and X. P. You. The international pulsar timing array project: using pulsars as a gravitational wave detector. *Classical and Quantum Gravity*, 27, November 2009.

[17] R. A. Hulse and J. H. Taylor. Discovery of a pulsar in a binary system. *Astrophys. J. Lett.*, 195:L51–L53, January 1975.

[18] B. Knispel, B. Allen, J. M. Cordes, J. S. Deneva, D. Anderson, C. Aulbert, N. D. R. Bhat, O. Bock, S. Bogdanov, A. Brazier, F. Camilo, D. J. Champion, S. Chatterjee, F. Crawford, P. B. Demorest, H. Fehrmann, P. C. C. Freire, M. E. Gonzalez, D. Hammer, J. W. T. Hessels, F. A. Jenet, L. Kasian, V. M. Kaspi, M. Kramer, P. Lazarus, J. van Leeuwen, D. R. Lorimer, A. G. Lyne, B. Machenschalk, M. A. McLaughlin, C. Messenger, D. J. Nice, M. A. Papa, H. J. Pletsch, R. Prix, S. M. Ransom, X. Siemens, I. H. Stairs, B. W. Stappers, K. Stovall, and A. Venkataraman. Pulsar Discovery by Global Volunteer Computing. *Science*, 329(5997):1305, September 2010.

[19] M. Kramer, I. H. Stairs, R. N. Manchester, M. A. McLaughlin, A. G. Lyne, R. D. Ferdman, M. Burgay, D. R. Lorimer, A. Possenti, N. D'Amico, J. M. Sarkissian, G. B. Hobbs, J. E. Reynolds, P. C. C. Freire, and F. Camilo. Tests of General Relativity from Timing the Double Pulsar. *Science*, 314(5796):97–102, October 2006.

[20] A. G. Lyne, M. Burgay, M. Kramer, A. Possenti, R. N. Manchester, F. Camilo, M. A. McLaughlin, D. R. Lorimer, N. D'Amico, B. C. Joshi, J. Reynolds, and P. C. C. Freire. A Double-Pulsar System: A Rare Laboratory for Relativistic Gravity and Plasma Physics. *Science*, 303(5661):1153–1157, February 2004.

[21] T. M. Niebauer, R. Schilling, K. Danzmann, A. Rüdiger, and W. Winkler. Nonstationary shot noise and its effect on the sensitivity of interferometers. *Physical Review A*, 43(9):5022–5029, May 1991.

[22] M. Prijatelj, H. Grote, J. Degallaix, M. Hewitson, S. Hild, C. Affeldt, A. Freise, J. Leong, H. Lück, K. A. Strain, H. Wittel, B. Willke, and K. Danzmann. Control and automatic alignment of the output mode cleaner of GEO 600. *Journal of Physics: Conference Series*, 228(1):012014+, May 2010.

[23] Volker Quetschke. Electro-Optic Modulators and Modulation for Enhanced LIGO and Beyond. In *Coherent Optical Technologies and Applications*, pages CMC1+. Optical Society of America, July 2008.

[24] Volker Quetschke, Qi-Ze Shu, Guido Mueller, David Reitze, and David Tanner. Complex Modulation. Technical Report T070197-00-R, LIGO Scientific Collaboration, University of Florida, August 2007.

[25] Bernard F. Schutz. Gravitational waves on the back of an envelope. *American Journal of Physics*, 52(5):412–419, 1984.

[26] J. R. Smith and for the LIGO Scientific Collaboration. The path to the enhanced and advanced LIGO gravitational-wave detectors. *Classical and Quantum Gravity*, 26(11):114013+, June 2009.

[27] R. L. Ward, R. Adhikari, B. Abbott, R. Abbott, D. Barron, R. Bork, T. Fricke, V. Frolov, J. Heefner, A. Ivanov, O. Miyakawa, K. McKenzie, B. Slagmolen, M. Smith, R. Taylor, S. Vass, S. Waldman, and A. Weinstein. DC readout experiment at the Caltech 40m prototype interferometer. *Classical and Quantum Gravity*, 25(11):114030+, 2008.

[28] Robert L. Ward. *Length Sensing and Control of an Advanced Prototype Interferometric Gravitational Wave Detector*. PhD thesis, California Institute of Technology, Pasadena, CA, February 2010.

[29] J. M. Weisberg and J. H. Taylor. The Relativistic Binary Pulsar B1913+16: Thirty Years of Observations and Analysis. In F.˜A.˜Rasio & I.˜H.˜Stairs, editor, *Binary Radio Pulsars*, volume 328 of *Astronomical Society of the Pacific Conference Series*, July 2005.

[30] Rainer Weiss. Electromagnetically Coupled Broadband Gravitational Antenna. *Quarterly Progress Reports of the Research Laboratory for Electronics*, 105:54–76, April 1972.